Iranian Journal of Materials Forming 10 (4) (2023) 45-51

Online ISSN: 2383-0042

Iranian Journal of Materials Forming

Journal Homepage: http://ijmf.shirazu.ac.ir

Research Article

An Analysis of Efficiency Parameter and its Modifications Utilized for Development of Processing Maps

H. Eskandari, M. Reihanian* and S.R. Alavi Zaree

Department of Materials Science and Engineering, Faculty of Engineering, Shahid Chamran University of Ahvaz, Ahvaz, Iran

ARTICLE INFO

Article history:

Received 18 February 2024
Reviewed 06 March 2024
Revised 07 March 2024
Accepted 08 March 2024

Keywords:

Metal forming
Hot deformation
Efficiency parameter
Dissipation map
Processing map

Please cite this article as:

Eskandari, H., Reihanian, M., & Alavi Zaree, S.R. (2023). An analysis of efficiency parameter and its modifications utilized for development of processing maps. *Iranian Journal of Materials Forming*, *10*(4), 45-51. https://doi.org/10.22099/IJMF.2024.49537.1283

ABSTRACT

The efficiency parameter, which is frequently utilized in the literature, can be expressed as η=(2m/m+1), where m is the strain rate sensitivity. The efficiency parameter is determined from a set of m values based on the strain rate and the temperature displayed in a three-dimensional map known as the power dissipation map. This method works if the test results for σ vs. $\dot{\varepsilon}$ at constant strain and temperature have a power-law distribution. Otherwise, it is incorrect to assess dissipation efficiency using the slope of the $ln\sigma - ln\dot{\varepsilon}$ graph. The present study proposes additional adjustments to the existing ones suggested in the literature for the prior technique by offering a scheme for evaluating η. Power dissipation maps for different techniques are developed at strains of 0.2 and 0.7 using X80 steel as a model material. In spite of the fact that the approaches rely on different assumptions and that there are differences in the temperature and strain rate at which the dissipation efficiency peak appears, there are some similarities in the power dissipation maps of all approaches when they are compared at different strains. In conclusion, although the conventional approach is erroneous, it is the most feasible and straightforward one.

1. Introduction

An important goal in hot deformation is to effectively manage the microstructure of the product, ensuring the absence of any micro- or macro flaws or flow instabilities [1]. The processing map is created to address this problem and serves as a clear depiction of how a material responds to the process parameters in terms of microstructural mechanisms [2, 3]. It is composed of a combination of a power dissipation map and an instability map and is used to examine the hot workability of various alloy systems such as steels [4], superalloys [5] and Ti alloys [6]. The formulation of these maps is based on the Dynamic Materials Model (DMM) utilized for the creation of processing maps in metal-processing systems [7]. A workpiece that heats up is considered a power dissipator.

* Corresponding author
E-mail address: m.reihanian@scu.ac.ir (M. Reihanian)
https://doi.org/10.22099/IJMF.2024.49537.1283

The constitutive equation for the workpiece material describes the variations of flow stress with process factors, such as temperature and strain rate. Two complementary components make up the total power dissipated: J co-content, which represents the dissipation through metallurgical processes, and G content, which represents the temperature rise. The power P (per unit volume) absorbed by the workpiece during plastic flow at any given strain rate is given by [7]:

$$p = \sigma.\dot{\varepsilon} = \int_0^{\dot{\varepsilon}} \sigma.d\dot{\varepsilon} + \int_0^{\sigma} \dot{\varepsilon}.d\sigma \quad (1)$$

or

$$p = G + J \quad (2)$$

The power partitioning between J and G at any given temperature and strain is just the material's strain-rate sensitivity as determined by:

$$m = \left(\frac{\partial ln\sigma}{\partial ln\dot{\varepsilon}}\right) \quad (3)$$

It follows from Eq. (3) that the dynamic constitutive equation is of the following type:

$$\sigma = C\dot{\varepsilon}^m \quad (4)$$

J is calculated at each deformation temperature by integrating Eq. (5) and, when paired with Eq. (4):

$$J = \int_0^{\sigma} \dot{\varepsilon}.d\sigma = \frac{\sigma.\dot{\varepsilon}.m}{m+1} \quad (5)$$

The flow stress and the strain rate-sensitivity factor m can be used to estimate the value of J at a specific temperature and strain rate using Eq. (5). The workpiece serves as a linear dissipator, and the value of J reaches its maximum at m = 1. Thus:

$$J_{max} = \frac{\sigma.\dot{\varepsilon}}{2} \quad (6)$$

If the power-dissipation capacity of the workpiece is stated in terms of efficiency of dissipation, η, which is defined as the ratio of J to J_{max}, the effect of J on the plastic flow of materials may be shown. It is evident from Eqs. (5) and (6) that:

$$\eta = \frac{J}{J_{max}} = \frac{2m}{m+1} \quad (7)$$

A third order polynomial can be used to fit the relationship between $ln\sigma$ and $ln\dot{\varepsilon}$ as below [8]:

$$ln\sigma = a + b(ln\dot{\varepsilon}) + c(ln\dot{\varepsilon})^2 + d(ln\dot{\varepsilon})^3 \quad (8)$$

The strain-rate sensitivity can be determined using Eq. (8) as follows:

$$m = \left(\frac{\partial ln\sigma}{\partial ln\dot{\varepsilon}}\right) = b + 2c(ln\dot{\varepsilon}) + 3d(ln\dot{\varepsilon})^2 \quad (9)$$

The first approach, which is widely used in the literature, bases the calculation of the efficiency of dissipation on Eq. (7). This equation is valid under the condition that the test data of σ vs. $\dot{\varepsilon}$ for a constant temperature and strain adhere to the power-law distribution described in Eq. (4). Otherwise, using the slope of the $ln\sigma - ln\dot{\varepsilon}$ curve to evaluate η is erroneous. The reason for the error when utilizing the conventional approach is that Eq. (7) in this approach assumes that m and, by extension, η, are independent of strain rate. In other words, applying Eq. (7) is only appropriate if the test data of σ vs. $\dot{\varepsilon}$ for a constant T and ε follow the power-law distribution, based on the assumption that m is constant. Therefore, it is incorrect to use the slope of the $ln\sigma - ln\dot{\varepsilon}$ curve, which gives a strain rate dependent m value, to evaluate η. Ebrahimi and Najafizadeh [9] solved this issue and modified the approach by considering the dissipation efficiency as follows:

$$\eta = \frac{\frac{m\dot{\varepsilon}_{min}^{m+1}}{m+1} + \int_{\dot{\varepsilon}_{min}}^{\dot{\varepsilon}} m\dot{\varepsilon}^m.d\dot{\varepsilon}}{\frac{\dot{\varepsilon}^{m+1}}{2}} \quad (10)$$

In the first term, m is considered constant and is determined by the slope of the $ln\sigma - ln\dot{\varepsilon}$ curve at $\dot{\varepsilon} = \dot{\varepsilon_{min}} = 10^{-2}$ s^{-1}. In the second term, m is varied with $\dot{\varepsilon}$. Trapezoidal rules can be used to calculate the integral in the second term. In an alternative approach, Narayana Murty et al. [10] suggested using a cubic spline to calculate the integral for G from the test data. The efficiency is then provided as follows:

$$\eta = \frac{\sigma.\dot{\varepsilon} - \int_0^{\dot{\varepsilon}} \sigma.d\dot{\varepsilon}}{\frac{\sigma.\dot{\varepsilon}}{2}} = 2\left(1 - \frac{\int_0^{\dot{\varepsilon}} \sigma.d\dot{\varepsilon}}{\sigma.\dot{\varepsilon}}\right) \quad (11)$$

Using a cubic spline fit has the benefit of producing more data points, which is helpful for assessing the integrals using the trapezoidal method. This method fits the continuous piecewise polynomial for the $\sigma - \dot{\varepsilon}$ data; σ is then obtained from this curve for any $\dot{\varepsilon}$, as needed in the assessment of the integral in Eq. (9).

In summary, the method that is frequently used in the literature to get the efficiency parameter is Eq. (7). It assumes a power-law distribution and erroneously evaluates η by using the slope of the $ln\sigma - ln\dot{\varepsilon}$ curve. Ebrahimi and Najafizadeh [9], and Narayana Murty et al. [10] address this problem by proposing Eq. (10) and

Eq. (11) as alternatives to Eq. (7) for the efficiency parameter, aiming to improve efficiency. In addition to the mentioned modifications to the efficiency parameter, Kim and Jeong [11] attempted to construct processing maps using creep mechanism equations, predict the effect of material constants, grain size on the power dissipation efficiency and the onset of flow instability. The developed processing maps were compared with the processing maps constructed using a conventional method, and the usefulness and limitation of this proposed approach were discussed. Furthermore, Rieiro et al. [12] presented a novel approach to stability conditions by taking into account equations that identify more and less stable regions, in contrast to previous authors, who deal with stable and nonstable regions. By employing their method, every measured point is adjusted to a hyperbolic sine equation, which is then used to compute parameters such as m and η for every strain rate and temperature. In this work, further modifications to earlier methods that were used to calculate the efficiency parameter are incorporated. The material used for analysis is X80 steel, which serves as a representative material. Power dissipation maps are then constructed at stresses of 0.2 and 0.7. The findings highlight the disparities in assessing efficiency indicators through the comparison of different methodologies.

2. Experimental Procedure

The study involved creating cylindrical compression samples with a height of 10 mm and a diameter of 7 mm from rolled plates of X80 API steel. A Zwick Z250 machines with 250 kN maximum load capacities and a graphite sheet as a lubricant was used for compression testing. The samples were heated to 1200 ºC, held for 10 minutes, and cooled to the deformation temperature. A range of strain rates (0.001, 0.01, 0.1, and 1 s^{-1}) and deformation temperatures (950, 1000, 1050, and 1100 ºC) were used in the hot compression testing. To ensure DRX presence, samples were crushed to a true strain of 0.7 and quenched in water.

The present work has received more changes compared to the prior approaches used for efficiency parameter. As an alternative approach, this method considers the dependency of the parameter C on the strain rate, rather than assuming it to be a constant value. The third-order polynomial function (Eq. (8)) is used to find the parameter C as a function of $\dot{\varepsilon}$. The intercept of the slope of tangent to $ln\sigma - ln\dot{\varepsilon}$ curve can be calculated to find the parameter C at a particular $\dot{\varepsilon}$ as below:

$$C = \exp(ln\sigma - mln\dot{\varepsilon}) \tag{12}$$

Eq. (10) is altered to Eq. (13) by incorporating a C value, which, similar to m, is dependent on the strain rate.

$$\eta = \frac{C\frac{m\dot{\varepsilon}_{min}^{m+1}}{m+1} + \int_{\dot{\varepsilon}_{min}}^{\dot{\varepsilon}} Cm\dot{\varepsilon}^{m}.d\dot{\varepsilon}}{C\frac{\dot{\varepsilon}^{m+1}}{2}} \tag{13}$$

Another change is to use the third order polynomial Eq. (8) to construct the integral in Eq. (11) rather than a cubic spline fit to the $\sigma - \dot{\varepsilon}$ data. In order to evaluate and contrast different techniques, an X80 steel is employed as a representative material. The power dissipation map generated by various approaches is then developed at two strain rates 0.2 and 0.7. The results of each approach are compared and analyzed. A synopsis of the concepts and presumptions of the several methods used to determine the dissipation efficiency is presented in Table 1.

Table 1. A synopsis of the concepts and presumptions of the several methods used to determine the dissipation efficiency

Appr.	Formulation of η	Constitutive equation	Variability of η	Variability of m	Variability of C	Ref.
1	$\eta = \frac{J}{J_{max}} = \frac{2m}{m+1}$	$\sigma = C\dot{\varepsilon}^{m}$	Strain rate independent	Strain rate dependent	Constant	[1]
2	$\eta = \frac{\frac{m\dot{\varepsilon}_{min}^{m+1}}{m+1} + \int_{\dot{\varepsilon}_{min}}^{\dot{\varepsilon}} m\dot{\varepsilon}^{m}.d\dot{\varepsilon}}{\frac{\dot{\varepsilon}^{m+1}}{2}}$	$\sigma = C\dot{\varepsilon}^{m}$	Strain rate dependent	Strain rate dependent	Constant	[9]
3	$\eta = \frac{C\frac{m\dot{\varepsilon}_{min}^{m+1}}{m+1} + \int_{\dot{\varepsilon}_{min}}^{\dot{\varepsilon}} Cm\dot{\varepsilon}^{m}.d\dot{\varepsilon}}{C\frac{\dot{\varepsilon}^{m+1}}{2}}$	$\sigma = C\dot{\varepsilon}^{m}$	Strain rate dependent	Strain rate dependent	Strain rate dependent	Current work (modification to [9])
4	$\eta = 2(1 - \frac{\int_0^{\dot{\varepsilon}} \sigma.d\dot{\varepsilon}}{\sigma.\dot{\varepsilon}})$	Third order polynomial fit to $ln\sigma - ln\dot{\varepsilon}$ data	Strain rate dependent	Strain rate dependent	Not applicable	Current work (modification to [10])

3. Results and Discussion

Fig. 1 and Fig. 2 illustrate the power dissipation maps derived at strain levels of 0.2 and 0.7, respectively, using the different methodologies previously addressed. The three-dimensional power dissipation map at strain of 0.7 for the approaches 3 and 4 presented in the current work is illustrated in Fig. 3. The findings show that although there are some variations in the peak efficiency and the temperature and strain rate regime where the peak efficiency occurs, the overall distribution of the efficiency parameter is similar. Tables 2 and 3 contain specifics about the peak efficiencies of the different techniques, as well as information about the temperature and strain rate regimes at a strain of 0.2 and 0.7. At strain of 0.2, approaches 1, 2, and 3 show a peak value of 0.3, whereas approach 4 shows a peak value of 0.35 at the same temperature range of 980–1015 ºC with a similar strain rate range of 0.001-0.002 s^{-1}. In the temperature range of 1080-1100 ºC and strain rate range of 0.001-0.002 s^{-1}, approach 1 and 3 exhibit an additional peak of 0.4. In the temperature range of 1020–1100 ºC and strain rate range of 0.001-0.009 s^{-1}, approach 2 displays a peak of 0.45. Approach 4 similarly shows the same peak value, but it does so in the 1090–1100 ºC temperature range and the 0.001-0.003 s^{-1} strain rate range. At a strain of 0.7, all approaches exhibit a peak of 0.25 within the temperature range of 950-980 ºC and strain rate range of 0.001-0.015 s^{-1} (approaches 1 and 2), and within the strain rate range of 0.001-0.022 s^{-1} (approaches 3 and 4). Approach 1, 2, and 3 exhibit an additional peak of 0.25 in the temperature range of 1025-1100 ºC, along with different strain rate ranges. Approach 4 exhibits a maximum value of 0.3 within the temperature range of 1080-1100 ºC and the strain rate range of 0.001-0.003 s^{-1}. When comparing various methods at different strains, it is evident that while certain approaches are based on different assumptions, there is a general resemblance in the power dissipation maps of all approaches. The dissipation efficiency peak varies in terms of the temperature and strain rate at which it occurs, as well as its peak value. An alternative way of comparing the different approaches is to plot the variation in efficiency

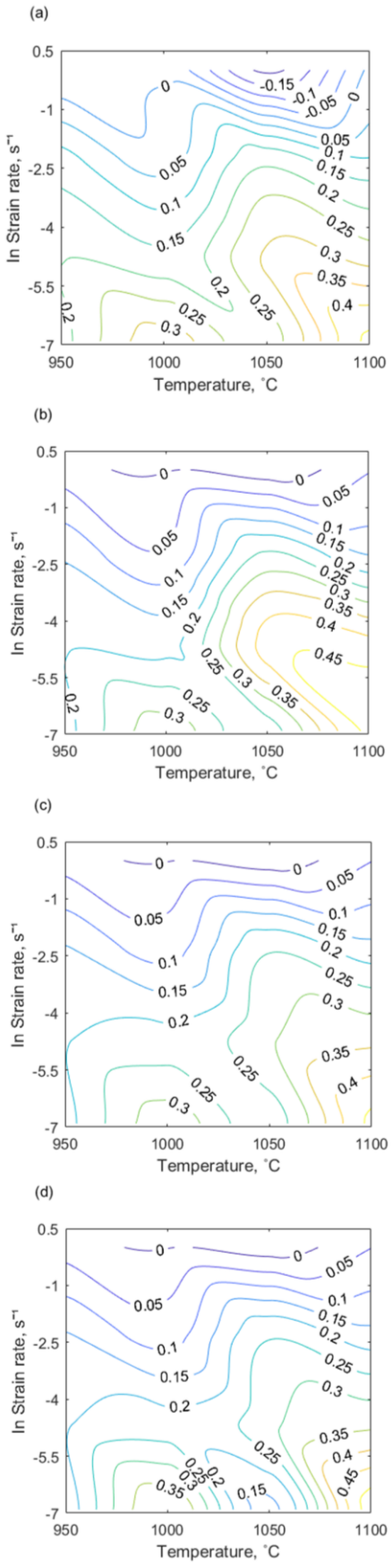

Fig. 1. Power dissipation map for (a) approach 1, (b) approach 2, (c) approach 3 and (d) approach 4 at strain of 0.2.

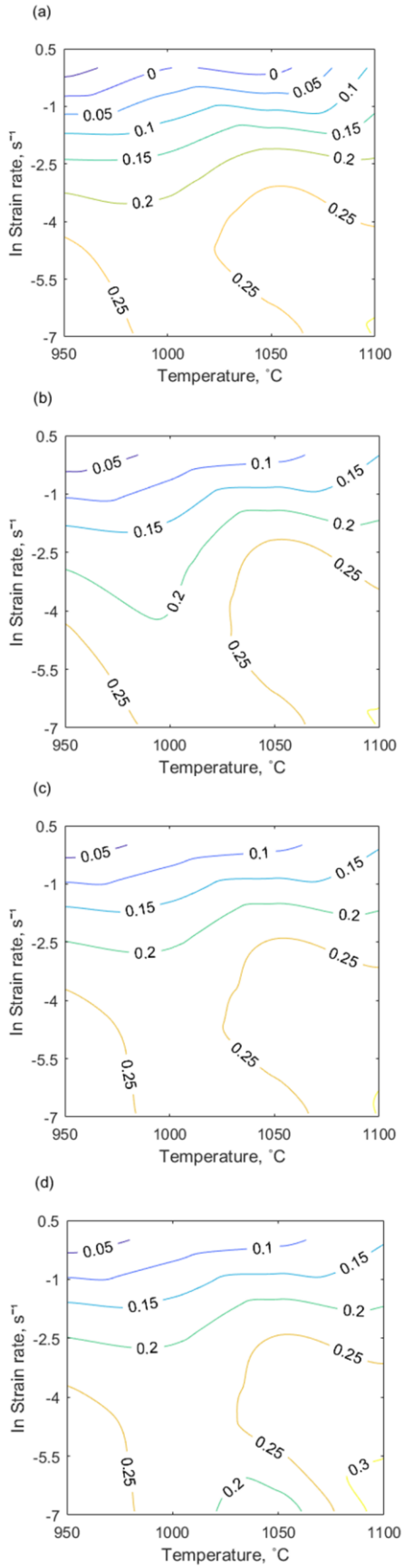

Fig. 2. Power dissipation map for (a) approach 1, (b) approach 2, (c) approach 3 and (d) approach 4 at strain of 0.7.

against the strain rate at different testing temperatures (Fig. 4). It is observed from the data that the efficiency values vary to some degree at different strain rates. This is primarily attributed to the assumptions made by various methodologies. The relationship between the efficiency parameter, strain rate, and temperature is due to the power dissipation that happens as a result of microstructural changes in the material. This relationship can be represented as a power dissipation map. They display distinct domains that are associated with specific microstructural processes. For instance, the maximum efficiency ranges from 30-35%, 40%, and 50-55% for materials with low, medium, and high stacking fault energy, respectively [9]. Higher efficiency parameters can be achieved by the processes of super plasticity and cracking. The 3D dissipation map reveals that the efficiency parameter is represented as a surface in 3D space, exhibiting peaks at different temperature and strain rate ranges. Thus, in specific circumstances, it reduces with a rise in strain rate, while in other cases, it grows, and under certain conditions, it reaches a maximum point. Hence, the efficiency parameter of X80 steel exhibits a decline with increasing strain rate at temperatures of 950 °C and 1100 °C, but reaches its peak at temperatures of 1000 °C and 1050 °C.

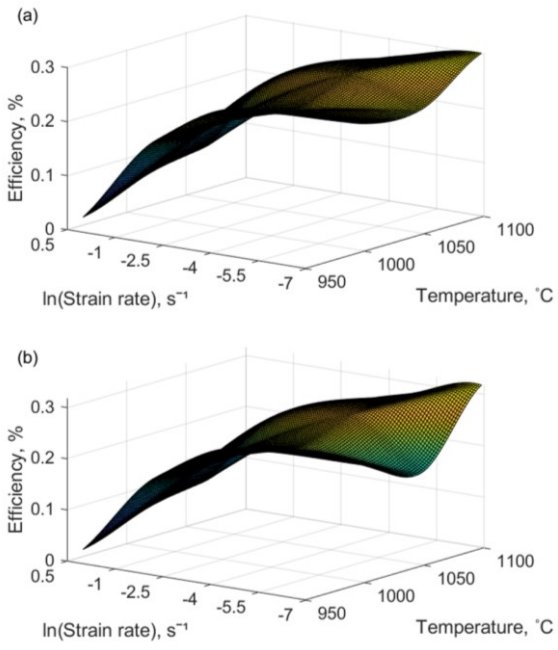

Fig. 3. Three-dimensional power dissipation map for (a) approach 3 and (b) approach 4 at strain of 0.7.

Table 2. Peak values of the dissipation efficiency and the corresponding temperature and strain rate ranges for various approaches at strain of 0.2

Approach	**Strain=0.2**					
	Peak value	T (ºC)	$\dot{\varepsilon}$ (s^{-1})	Peak value	T (ºC)	$\dot{\varepsilon}$ (s^{-1})
1	0.3	980-1015	0.001-0.002	0.4	1080-1100	0.001-0.002
2	0.3	980-1015	0.001-0.002	0.45	1020-1100	0.001-0.009
3	0.3	980-1015	0.001-0.002	0.4	1080-1100	0.001-0.002
4	0.35	980-1015	0.001-0.002	0.45	1090-1100	0.001-0.003

Table 3. Peak values of the dissipation efficiency and the corresponding temperature and strain rate ranges for various approaches at strain of 0.7

Approach	**Strain=0.7**					
	Peak value	T (ºC)	$\dot{\varepsilon}$ (s^{-1})	Peak value	T (ºC)	$\dot{\varepsilon}$ (s^{-1})
1	0.25	950-980	0.001-0.015	0.25	1025-1100	0.001-0.03
2	0.25	950-980	0.001-0.015	0.25	1025-1100	0.001-0.09
3	0.25	950-980	0.001-0.022	0.25	1025-1100	0.001-0.08
4	0.25	950-980	0.001-0.022	0.3	1080-1100	0.001-0.003

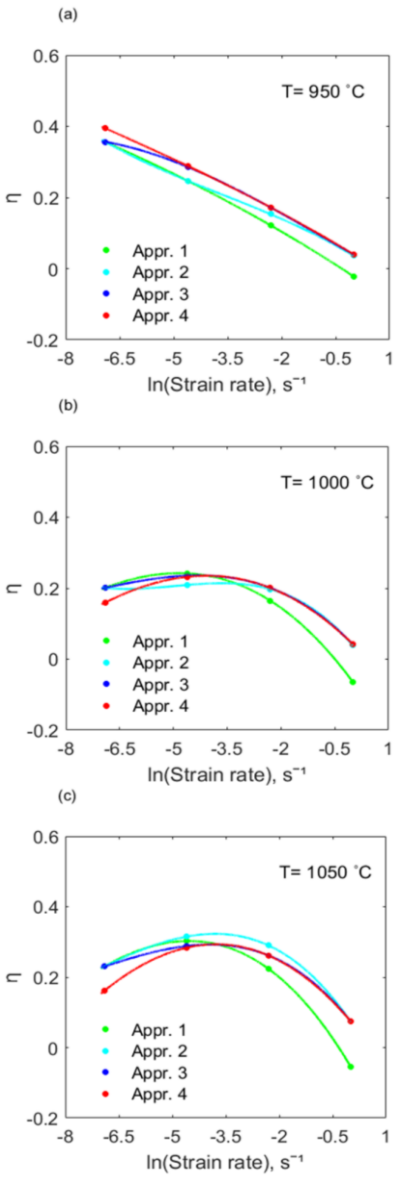

Fig. 4. Variation in the efficiency parameter with the strain rate at different temperatures.

4. Conclusion

This paper discusses the conventional approach to calculate the efficiency parameter and how it has been modified. Additional modification has been made to the previous methods used for calculating the efficiency parameter. The material chosen for analysis is X80 steel, which is regarded as a typical material. Subsequently, power dissipation maps are generated at strain levels of 0.2 and 0.7.

The dissipation maps of different methods exhibit slight variations in peak efficiency, strain rate and, temperature ranges. At a strain of 0.2, approaches 1, 2, and 3 show a peak value of 0.3, while approach 4 shows a peak value of 0.35 at 980-1015 °C and 0.001-0.002 s^{-1}. At a strain of 0.7, all approaches show a maximum peak

value of 0.25 within the same temperature range, with the strain rate range varying between approaches 1 and 2 and methods 3 and 4.

Although the approaches are based on different assumptions and exhibit variations in temperature and strain rate where the dissipation efficiency peak occurs, there are similarities in the power dissipation maps of all approaches when compared at various strains. To summarize, although the conventional method has errors, it is feasible and the most straightforward.

Acknowledgments

The funding of Shahid Chamran University of Ahvaz through grant number *SCU.EM1401.375* is gratefully appreciated.

Credit authorship contribution

H. Eskandari: investigation, formal analysis, methodology, validation. M. Reihanian: supervision, conceptualization, writing original draft, visualization. S.R. Alvai Zaree: supervision.

Conflict of Interests

The authors have no relevant financial or non-financial interests to disclose.

Funding

This research was funded by Shahid Chamran University.

5. References

[1] Prasad, Y. V. R. K., & Seshacharyulu, T. J. M. R. (1998). Modelling of hot deformation for microstructural control. *International Materials Reviews*, *43*(6), 243-258. https://doi.org/10.1179/imr.1998.43.6.243

[2] Prasad, Y. V. R. K. (2003). Processing maps: A status report. *Journal of Materials Engineering and Performance*, *12*, 638-645. https://doi.org/10.1361/105994903322692420

[3] Narayana Murty, S. V. S., Nageswara Rao, B., & Kashyap, B. P. (2000). Instability criteria for hot deformation of materials. *International Materials Reviews*, *45*(1), 15-26. https://doi.org/10.1179/095066000771048782

[4] Pu, E., Zheng, W., Xiang, J., Song, Z., & Li, J. (2014). Hot deformation characteristic and processing map of superaustenitic stainless steel S32654. *Materials Science and Engineering: A*, *598*, 174-182. https://doi.org/10.1016/j.msea.2014.01.027

[5] Cai, D., Xiong, L., Liu, W., Sun, G., & Yao, M. (2009). Characterization of hot deformation behavior of a Ni-base superalloy using processing map. *Materials & Design*, *30*(3), 921-925. https://doi.org/10.1016/j.matdes.2008.05.006

[6] Luo, J., Li, M., Yu, W., & Li, H. (2009). Effect of the strain on processing maps of titanium alloys in isothermal compression. *Materials Science and Engineering: A*, *504*(1-2), 90-98. https://doi.org/10.1016/j.msea.2008.10.020

[7] Prasad, Y. V. R. K., Gegel, H. L., Doraivelu, S. M., Malas, J. C., Morgan, J. T., Lark, K. A., & Barker, D. R. (1984). Modeling of dynamic material behavior in hot deformation: Forging of Ti-6242. *Metallurgical Transactions A*, *15*, 1883-1892. https://doi.org/10.1007/BF02664902

[8] Huang, H. Q., Di, H. S., Yan, N., Zhang, J. C., Deng, Y. G., Misra, R. D. K., & Li, J. P. (2018). Hot deformation behavior and processing maps of a high Al-low Si transformation-induced plasticity steel: microstructural evolution and flow stress behavior. *Acta Metallurgica Sinica (English Letters)*, *31*, 503-514. https://doi.org/10.1007/s40195-017-0676-2

[9] Ebrahimi, R., & Najafizadeh, A. (2004). Optimization of hot workability in Ti-IF steel by using the processing map. *International Journal of Iron & Steel Society of Iran*, *1*(1), 1-7.

[10] Murty, S. V. S. N., Sarma, M. S., & Rao, B. N. (1997). On the evaluation of efficiency parameters in processing maps. *Metallurgical and Materials Transactions A(USA)*, *28*(7), 1581-1582. https://doi.org/10.1007/s11661-997-0219-y

[11] Kim, W. J., & Jeong, H. T. (2020). Construction of processing maps combined with deformation mechanism maps using creep deformation equations. *Journal of Materials Research and Technology*, *9*(6), 13434-13449. https://doi.org/10.1016/j.jmrt.2020.09.023

[12] Rieiro, I., Carsí, M., & Ruano, O. A. (2017). A new stability criterion for the hot deformation behavior of materials: application to the AZ31 magnesium alloy. *Metallurgical and Materials Transactions A*, *48*(7), 3445-3460. https://doi.org/10.1007/s11661-017-4102-1